Various far-field hydrological responses during 2015 Gorkha earthquake at two distant wells

Xudong Huang
Wuhan University

Yu Zhang (yuzhang@sgg.whu.edu.cn)
Wuhan University https://orcid.org/0000-0002-8528-7746

Full paper

Keywords: earthquake, water level, coherence, tidal response, transmissivity

Posted Date: November 11th, 2020

DOI: https://doi.org/10.21203/rs.3.rs-45283/v2

Version of Record: A version of this preprint was published at Earth, Planets and Space on May 31st, 2021. See the published version at https://doi.org/10.1186/s40623-021-01441-0.

Various far-field hydrological responses during 2015 Gorkha earthquake at two distant wells

by

[1]Xudong Huang
[1,2]Yu Zhang

1School of Geodesy and Geomatics

Wuhan University

Wuhan, 430079, China

2Key Laboratory of Geospace Environment and Geodesy

Ministry of Education

Wuhan, 430079, China

Corresponding Author:

*Yu Zhang (yuz124@gmail.com or yuzhang@sgg.whu.edu.cn)

Submitted for consideration of publication in
Earth, Planet and Space
July 12, 2020
Revised and resubmitted for consideration of publication in
Earth, Planet and Space
Sept 27, 2020

Abstract

Aquifer hydraulic parameter can change during earthquakes. Continuous monitoring of the response of water level to seismic waves or solid Earth tides provides an opportunity to document how earthquakes influence hydrological properties. Here we use data of two groundwater wells, Dian-22 (D22) and Lijiang (LJ) well, in southeast Tibet Plateau in response to the 2015 Mw 7.8 Gorkha earthquake to illustrate hydrological implications. The coherences of water level and seismic wave before and after the far-field earthquake show systematic variations, which may confirm the coseismic dynamic shaking influence at high frequencies (f > 8 cpd). The tidal response of water levels in these wells shows abrupt coseismic changes of both phase shift and amplitude ratio after the earthquake, which may be interpreted as an occurrence in the vertical permeability of a switched semiconfined aquifer in the D22 well, or an enhancement unconfined aquifer in the LJ well . Using the continuous transmissivity monitoring, we show that the possible coseismic response for about 10 days and instant healing after 10 days to the earthquake. Thus, the dynamic shaking during the Gorkha earthquake may have caused the short term aquifer responses by reopening of preexisting vertical fractures and later healing at epicentral distances about 1500 km.

Key word: earthquake, water level, coherence, tidal response, transmissivity

1. Introduction

It has been widely reported that earthquakes can cause various hydrological responses, such as changes in groundwater level (Roeloffs, 1998; Brodsky et al., 2003), increases in stream flow (Muir-Wood and King, 1993; Manga, 2001; Wang et al., 2004a; Wang and Manga, 2015), water-temperature variations (Mogiet al., 1989; Shi et al., 2007; Wang et al., 2013; Shi and Wang, 2014; Zeng et al., 2014; Ma, 2015) and chemical composition (Claesson et al., 2004; Skelton et al., 2014; Zeng et al., 2014), which are always interpreted by induced underground water transport (e.g., Claesson et al., 2007; Wang et al., 2013). Different mechanisms have been proposed to explain these coseismic transport enhancement, including changes in aquifer permeability or storativity (Rojstaczer et al.,1995; Wang et al., 2004a; Manga et al., 2012), static stress and dynamic stress induced pore pressure diffusion (Muir-Wood and King, 1993; Jonsson et al.,2003), consolidation/liquefaction of saturated sediments (Manga, 2001; Manga et al., 2003), rupturing and unclogging of fractures (Sibson and Rowland, 2003 Wang et al., 2004b), and water recharge tank (Kagabua et al., 2020). In phenomenological analysis of this underground flow, the coseismic change in permeability always can be adopted, which also usually attaches to horizontal flow in observation wells (Elkhoury et al., 2006; Xue et al., 2013; Shi et al., 2015) since permeability of a layered groundwater system in the horizontal direction is normally larger than that in the vertical direction (Liao et al., 2015). Recent studies show that near field and intermediate earthquakes may also breach the hydraulic barriers between aquifers and increase vertical permeability (Wang et al., 2004a; Shi and Wang, 2014; Shi and Wang, 2016; Wang et al., 2018; Zhang et al., 2019) that can explain some unexpected aquifer hydrological responses at near field observation.

Groundwater level monitoring plays an important part in the earthquake prediction program in China, and a nationwide groundwater monitoring well network has been constructed for this

purpose (Shi et al., 2015b). In this work, we examine the water level responses at the Dian-22 (D22) and Lijiang (LJ) wells at southeast margin of Tibet Plateau due to the 2015 Mw 7.8 Nepal Gorkha earthquake (Figure 1). The distant earthquake (> 1000 km) induced distinct coseismic water-level responses in these two adjacent wells at successive time. The D22 well may be caused by a large coseismic increase in the horizontal permeability; the other LJ well may be caused by a coseismic aquifer leakage switch, i.e., a seismic wave induced vertical diffusion by vertical permeability enhancement in this far field. We interpret the earthquake-induced changes using different moving window coherence with regards to seismic and atmospheric excitations to identify the time dependent hydrological responses in preseismic, coseimic and postseismic phases. Thus, the tidal responses of groundwater in these wells are interpreted by a horizontal flow and a vertical drainage in different time. Furthermore, we interpret the responses in terms of preexist factures unclogging and reclogging by seismic shaking during the earthquake and show that the local site amplification may favor effect on shallow hydrological systems at epicentral distances >1000 km.

2. Observations and data

The April 2015 Nepal Gorkha earthquake occurred at Main Himalayan thrust (MHT) for ~140 km east-west and ~50 km across strike and 80 km WNW of Kathmandu, with a hypocentral depth of ~15 km, the focal mechanism indicating thrusting on a sub-horizontal fault dipping at ~10^{o} north, which nucleated approximating to the brittle-ductile transition and propagated east along the MHT but did not rupture to the surface (see Figure 1; Avouac et al., 2015; Elliott et al., 2016).

We have collected the water level data from two distant wells with distinct coseismic responses to the earthquake located in the south boundary of the Tibet Plateau (also see Figure 1).

The D22 well is located near the center of Luxi Basin. According to drilling data, the well with 200.17 m depth is cased with pipe to 95.57 m, with a screened interval between 95.57 and 200.17 m. It is drilled with a diameter of 168 mm to 6.1 m, and with a diameter of 146 mm from 6.1 m to 56.84 m. The diameter between 56.84 m to 95.57m is 127mm, and at much deeper levels the well has no casing (see details in Figure 2a and Table 1). The LJ well be situated at the north end of Honghe (HH) fault zone, at the intersection of Lijiang-Jianchuan (LJ-JS) fault and Zhongdian-Dali (ZD-DL) fault (Feng et al., 2004). The well is drilled to 310 m and cased with pipe to 240 m, with a screened interval between 240 and 310 m. Within 20 m depth, the well diameter is 194 mm. And the diameter reduces to 166 mm at the depth of 80 m. At depth of 80 – 240 m the well diameter is 127 mm. The rest part of the well has the diameter of 108 mm (see details in Figure 2b and Table 1).

The water level is measured by an LN-3A digital water-level gauge (Institute of Seismic Science, China Earthquake Administration). It converts the reading of the digital pressure measurement into the groundwater level. The sampling is 1 min with the resolution of 1 mm, and the absolute accuracy is 0.2%. The along well seismic waves are recorded by the CTS-1 broad-band seismometer with sampling of 0.01 s. Seismic-wave and water-level data collected from April 9 to May 11 2015 are analyzed.

2. Coseismic response identifications

Preseismic, coseismic and postseismic water-level changes caused by the Gorkha earthquake are clearly identified in the seismic wave and water level data (Figures 3 and 4). The water-level responses show oscillations with sustained postseismic variation. We calculate the difference between the levels within 2 h after the origin time of the Gorkha earthquake to get the amplitude of the oscillation in each well (Ma and Huang, 2017). The amplitudes of the coseismic water level

changes are shown in Table 1 and Figures 1. The approximate durations of the coseismic water level changes (the recovery times) are also measured by when the water level decreases down to 5% of the maximum coseismic response.

Compared the seismic wave (Figure 3) with the water level (Figure 4), it is easy to distinguish the coseismic water level response to the Gorkha earthquake in the D22 well and LJ well by 0.76 m and 0.16 m respectively. The duration times of the coseismic water-level changes are 109 min and 97 min. By exact checking the seismic-wave and water-level time windows, we can discover that the coseismic water-level response mainly corresponds to the Rayleigh surface-wave arrival times (see Figures 3 and 4). These results suggest that the amplitudes and durations of the coseismic water-level changes were associated with teleseismic surface-wave oscillations.

3.1 Coseismic coherency analysis

To estimate how the seismic wave influences the water level, we first calculated the cross ordinary coherence functions γ_{xy}^2 among the water level, vertical velocity seismograms and barometric pressure for each station (Lai, et al., 2013). The ordinary coherence function is defined as

$$\gamma_{xy}^2 = \frac{\left|G_{xy}(\omega)\right|^2}{G_{xx}(\omega)G_{yy}(\omega)}, \quad (1)$$

where $G_{xx}(\omega)$ and $G_{yy}(\omega)$ are the power spectra of two signals respectively, and $G_{xy}(\omega)$ is the cross-power spectrum between them.

In the calculation, we used the data of each 3 days around the earthquake from April 23, 2015 to April 28, 2015. These data are continuous and stable. The time window and moving window are 1024 min and 512 min, respectively. We calculated the coherence before, around and after the earthquake origin time (Figures 5 and 6). Previous studies show that the barometric pressure and

Earth tide are two persistent factors affecting the water level change (e.g., Lai et al., 2013). Because barometric pressure is one of the factors of well water level change, the coseismic influence of seismic wave on well water level may be contaminated by it. We must exclude the possibility that barometric pressure has influence on the coseismic seismic wave, so as to determine the sufficient coseismic relationship between seismic wave and water level. And the great transfer efficiency of semidiurnal tide for water level located around 1 - 8 cpd. In the low-frequency band (f < 1 cpd), the barometric pressure also show the great transfer efficiency for most wells whose ordinary coherence functions were up to 0.9. In the high-frequency band (f > 8 cpd), both efficiencies for water level decreased though (Lai, et al., 2013). However, in the D22 well, we can observe the high efficiencies for barometric pressure, which may be caused by the in-well barometer. The coseismic shaking broke this high coherence in this high-frequency band (Figure 5c second panel), while the water level response to velocity show the coherence enhancement between the preseismic and postseismic stages (see Figures 5a, second panel). At the postseismic stage, the low frequency (f < 8 cpd) transfer efficiencies of velocity increments (up to 0.7) of semidiurnal tide for water level and barometric pressure which may mean in-phase responses of the semidiurnal tides and post seismic hydrological recovery. The coseismic coherence of barometric pressure and vertical velocity show little downward at high frequencies. In the low frequency band, the increased coherence may represent the tide transfer efficiencies in the both time series. In the LJ well, we can observe the similar water level in response to the velocity excited by the seismic waves at different stages (Figure 6a). The barometric pressure transfer efficiencies of water level did not show obvious coseismic change as mainly affected in the 1 - 8 cpd (Figure 6c), as previous mentioned (Lai et al., 2013). It is noted that the coherence between the velocity and barometric pressure show the similar coseismic decrease in the high frequency band (f > 8 cpd) as that between

the water level and barometric pressure in the D22 well (comparing Figures 5c and 6b). An open well barometric pressure and seismic wave observation may make this correspondence. The relative high coherence except the coseismic stage may come from the wind noise. In short, the Gorkha earthquake coseismic responses directly may shake in high frequency band (f > 8 cpd), and further switched the low frequency semidiurnal tide transfer efficiencies (1 - 8 cpd), which further illustrate far field the hydrological responses to the great earthquake.

3.2 Aquifer tidal response analysis

Among the tidal constituents, O1 and M2 tides have large amplitudes and with low barometric effect. Therefore, they are the constituents most widely used in tidal analysis (e.g., Zhang et al., 2016; Wang et al., 2019). M2 tide is more popular for its higher accuracy at 12.42 hour period (Hsieh et al., 1987; Rojstaczer and Agnew 1989; Doan et al., 2006), which we use for the following tide analysis.

The amplitude and phase responses of water level to M2 tide can reflect aquifer storativity and permeability around well (Hsieh et al., 1987; Elkhoury et al., 2006; Doan et al., 2006; Xue et al., 2013). In a confined system, high permeability usually causes small phase lags, whereas low permeability results in large phase lags. The amplitude response is primary to measure specific storage (Zhang et al., 2016).

According to Cooper et al. (1965) the steady fluctuation of water level in a well occurs at the same frequency as the harmonic pressure head disturbance in the aquifer which however leads to different amplitude and phase shift. Hsieh et al. (1987) described the pressure head disturbance and water-level response as

$$h_f = h_0 \exp(i\omega t), \tag{2}$$

$$x = x_0 \exp(i\omega t), \tag{3}$$

where h_f express the fluctuating pressure head in the aquifer. h_0 is the complex amplitude of the pressure head fluctuation. x is the water level from the static position. x_0 is the complex amplitude of the water-level fluctuation. *t* indicates time. $\omega = 2\pi/\tau$ is the frequency of fluctuation, where τ is the period of fluctuation. The ratio between the amplitude of the water-level fluctuation and that of the pressure head fluctuation defines the amplitude response *A* as

$$A = |x_0/h_0|, \tag{4}$$

The phase shift is defined as

$$\eta = \arg\,(x_0/h_0), \tag{5}$$

where arg() is the argument of a complex number.

M2 tidal signal was decomposed by Bayesian statistics (Tamura *et al.*, 1991). Steps and spikes caused by instrument malfunctions or maintenance work were removed before the analysis. The barometric correction was performed by local barometric data. We used the data from April 9 to May 11 in 2015 when there were no other large earthquakes. The 10-day time window was selected to determine the amplitude and phase responses, since Elkhoury et al. (2006) used 200 or 240 hour time window to differentiate the M2 and S2 tidal constituents. In Figures 7 and 8, the blue error bars indicate the root-mean-square error (RMSE) of the tidal analysis. The phase shift transient increase caused by the Gorkha earthquake in two wells can be clearly distinguished. The phase shifts of the tidal response of water level increased after the earthquake in both wells consistent to the time dependent coherence analysis. Near zero phase before the earthquake became positive after the earthquake for the D22 well (from 0° to 10°). While the positive phase before the earthquake became more positive after the earthquake for the LJ well (from 7° to 9°), and restored at the postseismic phase.

4. Mechanisms for the water level variations during the earthquake

Many studies have applied the tidal response of the water level to study the permeability change of well-aquifer systems (Elkhoury et al., 2006; Xue et al., 2013; Lai et al., 2014; Shi and Wang, 2014; Yan et al., 2014; Shi et al., 2015; Zhang et al., 2019).The most common method used for permeability change estimation from tidal analysis was demonstrated by Hsieh et al. (1987). For a homogeneous, isotropic, laterally extensive, and confined aquifer, the phase shifts between Earth tides and water level are assumed to be caused by the time required for the water to flow into and out of the well, related the aquifer properties. In this case, the drainage effect of groundwater level is ignored and the resulting phase shift should always be negative due to the time required for water to horizontally flow. The near zero phase shift in the D22 well sometimes show negative value, which may be interpreted by this model (Elkhoury et al., 2006). For the positive phase shifts observed coseismicly in the D22 well and in the LJ well, which mean preceding water level to tidal strain, Hsieh's model no longer suffices. Roeloffs (1996) presented another model in which vertical drainage of pore pressure to the water table can cause wave-level change in advance. Figure 7 shows that in the D22 well, the coseismic phase response changes to be positive and restores to be near zero gradually in postseimic stage. Thus, these phase responses are a combination of normal phase lag caused by wellbore storage effect (aquifer confined) and coseismic phase lead caused by pore diffusion (aquifer not well confined). These observed phase responses can be considered a measure of permeability for either horizontal or vertical fluid flows (e.g., Lai et al., 2013, 2014).

4.1 Estimation of the aquifer property changes

The coseismic phase shift of the D22 well that varied from zero within 8° variation to be positive, could be interpreted a switched vertical diffusion (Shi et al., 2016). Nevertheless, the

preseismic and postseismic situations need to be identified. Based on Hsieh's horizontal flow model, the transmissivity T of aquifers can be estimated, which is the rate of water transmission through a unit width of aquifer under a unit hydraulic gradient as (Doan et al. 2006)

$$A = (E^2 + F^2)^{-1/2}, \tag{6}$$

$$\eta = -tan^{-1}(F/E), \tag{7}$$

where

$$E \approx 1 - (\omega r_c^2 2T)Kei(\alpha), \tag{8}$$

$$F \approx (\omega r_c^2/2T)Kei(\alpha), \tag{9}$$

$$\alpha = (\omega S/T)^{-1/2} r_w, \tag{10}$$

S is the dimensionless storage coefficient. *Ker* and *Kei* are the zero-order Kelvin functions. r_w is the radius of the well, and r_c is the inner radius of the casing. ω is the frequency of the tide. The r_w and r_c can be gotten from drilling data (Figure 2a). Finally, the horizontal T_h can be estimated in the D22 well of a confined aquifer above 10^{-4} m^2/s at the two stages (also see Zhang et al., 2019) . While in a vertical pore-pressure diffusion model with positive phase shift, the pressure spreads to the free surface, the amplitude of the tide disappears (Roeloffs, 1996). At the tidal frequencies, the skin length may exceed the depth of the shielding layer under where to measure the well pressure diffusion as (Shi and Wang, 2016)

$$\mathrm{D}\frac{\partial^2 p}{\partial z^2} + \mathrm{BK_u}\frac{\partial \varepsilon}{\partial t} = \frac{\partial p}{\partial t}, \tag{11}$$

$$\mathrm{p}\left(z \to \infty\right) = \mathrm{BK_u}, \tag{12}$$

$$p(z = 0) = 0, \tag{13}$$

where the solution can be written as

$$\mathrm{p(z,\omega)} = \mathrm{BK_u}\varepsilon\left(1 - e^{-(1+i)z/\sqrt{2D/\omega}}\right), \tag{14}$$

representing the pore-pressure fluctuation at depth z. B is Skempton's coefficient. K_u is the bulk modulus of the saturated rock under undrained conditions. ε is the change in the volumetric strain. D is the hydraulic diffusivity. With the relation $T_v = DS$, the vertical transmissivity T_v in the D22 well > 3×10^{-6} m^2/s. Considering the coherence between water level and barometric pressure was nearly 0.8 before and after the Gorkha earthquake, without distinct declinations, these results provide evidence that aquifer was confined both before and after the earthquake, which was also insensitive to changes in the horizontal transmissivity while T_h > 10^{-4} m^2/s. While the coseismic turned positive phase may mean the instant seismic wave induced vertical diffusion, which also broke the barometric efficiency in the high frequency band (see Figure 5c second panel).

The phase shifts of LJ well are all positive, which may indicate leakage to the water table interpreted with the unconfined aquifer model, especially the coseismic enhancement around the Gorkha earthquake. Although a hydrogeological background of layered aquifer-aquitard system may bring controversy, a surface hydrological estimation has justified the tide insensitive high horizontal transmissivity in the LJ well (Liao and Wang, 2018). Therefore, the vertical pore pressure diffusion model is applicable to interpreter the coseismic response in the LJ well.

5. Discussion and conclusions

For the D22 well, the coseismic positive phase shift from 0° to 10° (Figure 7) indicates vertical diffusion in a semiconfined well-aquifer system during the earthquake. It is indicated that the well-confined aquifer before the Gorkha earthquake became semiconfined after the earthquake shaking arrival. These shifts recovered at the 11th day after the earthquake. This switch may have been caused by a reopening of vertical fractures (Liao et al., 2015), which would reseal over time (Figure 7). The change of aquifer type lasted 10 days. That the 10-day sufficient permeability enhancement finished at the 11th day in the continuous transmissivity measurement, also means

an instant recovery (Figure 9). It is noted that the 10 days change represented the vertical reopening, and the successive meant the covariant change in successive days. The instant recovery can be interpreted as the high frequency seismic wave induced the tiny mineral particle unclogging movement in the narrow pore throat in possible vertical fractures in marl stone, hereafter minerals instantly reclogged by the vertical water diffusion without high frequency shaking.

For the LJ well, the phase shift of the response to M2 tide is positive and negatively correlated with the amplitude response (Figure 8), as the expected behaviors of unconfined aquifers. The water level in well is insensitive to the tides (Liao and Wang, 2018). We can infer that the Gorkha earthquake had little influence on aquifer confinement changes at the LJ well. The LJ well remained well unconfined during the earthquake. By the continuous monitor of the vertical transmissivity (T_v), the distinct enhancement 8 days after the earthquake can last 3 days (see Figure 10). The total recovery to the pre-seismic state also happened 11 days after the earthquake. The enhancement of the vertical transmissivity following the Gorkha earthquake may have been caused by the further unclogging of preexisting fractures due to the shaking of seismic waves, also followed by an instant recovery to the common state.

Many studies have documented these earthquake-induced water permeability switching and enhancement in the near field (epicentral distance < 1 rupture length) and intermediate field (Rojstaczer et al., 1995; Manga and Rowland, 2009; Manga et al., 2012; Shi and Wang, 2014; Wang and Manga, 2015; Shi and Wang, 2016; Wang et al., 2018). The postseismic healing or reclogging of fractures permeability will restore permeability (Xue et al., 2013; Shi and Wang, 2015). The epicentral distances for the Gorkha earthquake of the two wells are similar in far field (several times rupture length ~ 1500 km, see Table 1). Using the empirical seismic energy estimation as (Wang, 2007)

$$\log(r) = 0.48M - 0.33\log e\,(r) - 1.4, \quad (16)$$

where r is the actual epicentral distance in kilometers, M is the earthquake magnitude, and e is the seismic energy density (in Jm^{-3}). The seismic energy density at the D22 well was 3.4×10^{-3} Jm^{-3}, while at the LJ well was 2.8×10^{-3} Jm^{-3}, using this relation derived in southern California, which were not consistent to the peak ground velocity (PGV) estimated from the seismograms (Figure 3). The PGV at the LJ well was two orders of magnitude greater. However, the epicenter distance of it is longer (1530.9 km), and coseismic water-level response magnitude and duration was shorter (Figure 1 and Table 1). We also calculated the static strain caused by the Gorkha earthquake based on the Okada model (Lin and Stein, 2004; Toda et al., 2005; Zhang et al., 2017), which turns out to be about magnitude of 10^{-12} (positive for dilatation). It is too small to cause water level rise, indicating that the effects of static strain on the coseismic water level change in the far field are negligible. The water level changes may only be caused by dynamic strain induced by the seismic waves. We infer that the local site amplification effect may make these abnormal seismic responses, which may further differ the hydrological responses under different hydrological backgrounds. The main aquifer lithology of the LJ well is dolomitic limestone that is aquitard but more suitable for fracture development than the marl stone in the D22 well (e.g., Mavko et al., 2007). Under the rough estimation of seismic energy at the two wells, about 10^{-3} Jm^{-3} is capable of triggering different hydrological responses (Wang and Manga, 2010). Therefore, it is reasonable to deduce whether the vertical fracture became active and total healing at these two far field wells can be referred to the high frequency seismic waves. Aquifer-type change may occur at the D22 well. The unclogging and reclogging may represent the tiny mineral colloidal particle movement and accumulation in narrow pore throat induced by the less seismic energy during the earthquake (see Figure 3).

Comparing Figures 9 and 10, we can see instant healing process during about 10 day period after the Gorkha earthquake. At the D22 well, the aquifer-type change of the switched vertical transmissivity changed from 0 m^2/s to around 1×10^{-5} m^2/s after the earthquake and decreased further to 0 m^2/s of total vertical healing. The distinct vertical transmissivity changes induced by the earthquake in the LJ well lasted 10 days. The persistent vertical transmissivity changed from about 1.3×10^{-5} m^2/s to 1.7×10^{-5} m^2/s, but returned to 1.2×10^{-5} m^2/s as the preseismic stage. These decreases may have been caused by the partial blocking of preexisting fractures induced by the Gorkha earthquake, indicating that the local hydrogeological conditions (e.g., permeability, aquifer lithology, and fracture aperture) are important to the recovery process.

The coherence of water level and seismic wave indicated that the coseismic hydrogeological responses were induced by high frequency (f > 8 cpd) ground oscillations with the high dynamic seismic energy. The recoveries only lasted 10 days which also means high frequency impact did not make persistent change in aquifer system as reported after the 2011 Tohoku earthquake (see Zhang et al., 2019). With the observations of short time step, we can discover this short term change. The wells are distant (about 1500 km) to the epicenter, and they are all affected by the Tibet plateau geological evolution. The series far-field hydrogeological responses, especially a coseismic aquifer-type change to semiconfined, may be considered as a significant factor in earthquake fluid monitoring in the seismic active area to great earthquakes.

Availability of data and materials

The data used in this study can be applied from the National Earthquake Data Center of the China Earthquake Administration (http://earthquake.cn/).

Competing interests

The authors declare that they have no competing interests.

Funding

This research is financially supported by the National Natural Science Foundation of China (NSFC), under Grant No. 41774119), the special Fundamental Research Funds for the Central Universities (2042017kf0228) and Wuhan University Experiment Technology Project Funding (WHU-2019-SYJS-12).

Authors' contributions

XH and YZ carried out most of geologic investigation, data collection, and data pre-treatment. XH finished the calculation and analysis of coherence and tidal responses and calculated the transmissivities. YZ finished the coseismic hydrological analysis. XH and YZ conceived and coordinated the study, drafted and approved the manuscript.

Acknowledgments

We thank the China Earthquake Administration for providing the data used in this study.

Reference

Avouac, J.-P., Meng L., Wei S., Wang W., Ampuerao J.-P. (2015) Unzipping of the lower edge of the locked Main Himalayan Thrust during the 2015, Mw 7.8 Gorkha earthquake. Nat. Geosci. http://dx.doi.org/10.1038/NGEO2518.

Brodsky, E. E., Roeloffs E., Woodcock D., Gall I., Manga M. (2003), A mechanism for sustained groundwater pressure changes induced by distant earthquakes, J. Geophys. Res., 108(B8), 2390, doi:10.1029/2002JB002321.

Cooper, H.H., Bredhoeft J.D., Papdopulos I.S., Bennnett R.R. (1965) The response of well-aquifer systems to seismic waves. J Geophys Res 70: 3915–3926

Claesson, L., Skelton A., Graham C., Dietl C., Mörth M., Torssander P., Kockum I. (2004) Hydrogeochemical changes before and after a major earthquake, Geology, 32(8), 641–644.

Claesson, L., Skelton A., Grahem C., Mörth C.-M. (2007) The timescale and mechanism of fault sealing and water-rock interaction after an earthquake, Geofluids, 7, 427–440, doi:10.1111/j.1468-8123.2007.00197.x.

Deng, Q., Zhang P., Ran Y. (2006) Distribution of active faults in China (1:4000000). Science Press, Beijing

Doan, M.L., Brodsky E.E., Prioul R., Signer C. (2006) Tidal analysis of borehole pressure—a tutorial. Schlumberger Research Report

Elliott, J.R., Jolivet, R., Gonzalez, P.J., Avouac, J.-P., Hollingsworth, J.C., Searle, M.P., Stevens, V.L., (2016) Himalayan megathrust geometry and relation to topography revealed by the Gorkha earthquake. Nat. Geosci. http://dx.doi.org/10.1038/NGEO2623

Elkhoury, J.E., Brodsky E.E., Agnew D.C. (2006) Seismic waves increase permeability. Nature 411:1135–1138

Feng, W. P. et al. (2004) 'Analysis of the characteristic about the Honghe active fault zone based on the ETM+ remote sensing images', in International Geoscience and Remote Sensing Symposium (IGARSS). doi: 10.1109/igarss.2004.1370323.

Hsieh, P.A., Bredehoeft J.D., Farr J.M. (1987) Determination of aquifer transmissivity from earth tide analysis. Water Resour Res 23(10):1824–1832

Jonsson, S., Segall P., Pedersen R., Bjornsson G. (2003) Postearthquake ground movements correlated to pore-pressure transients, Nature, 424, 179–183, doi:10.1038/nature01776.

Kagabua, M., Ideb, K., Hosonoc, T., Nakagawaa, K., Shimadac, J., 2020. Describing coseismic groundwater level rise using tank model in volcanic aquifers, Kumamoto, southern Japan, J. Hydrology, 582, 124464.

Lai G., Huang F., Ge H. (2011) Apparent permeability variation of under-ground water aquifer induced by an earthquake: a case of the Zhouzhi well and the 2008 Wenchuan earthquake. Earthq Sci 24, 437–445.

Lai, G., Ge, H. and Wang, W. (2013) 'Transfer functions of the well-aquifer systems response to atmospheric loading and Earth tide from low to high-frequency band', Journal of Geophysical Research: Solid Earth, 118(5), pp. 1904–1924. doi: 10.1002/jgrb.50165.

Lai, G., Ge H., Xue L., Brodsky E. E., Huang F., and Wang W. (2014) Tidal response variation and recovery following the Wenchuan earthquake from water level data of multiple wells in the near field, Tectonophysics, 619-620, 115–122.

Liao, X., Wang C. Y., Liu C. P. (2015) Disruption of groundwater systems by earthquakes, Geophys. Res. Lett., 42, 9758–9763.

Liao, X., & Wang, C.-Y. (2018). Seasonal permeability change of the shallow crust inferred from deep well monitoring. Geophysical Research Letters, 45, 11,130–11,136. https://doi.org/10.1029/2018GL080161

Lin, J., Stein, R.S., (2004) Stress triggering in thrust and subduction earthquakes and stress interaction between the southern San Andreas and nearby thrust and strike slip faults. J. Geophys. Res. 109, B02303.

Marine, I. W. (1975) Water level fluctuations due to earth tides in a well pumping from slightly fractured crystalline rock, Water Resources Research, 11, doi: 10.1029/WR011i001p00165.

Ma, Y., (2015) Earthquake-related temperature changes in two neighboring hot springs at Xiangcheng, China. Geofluids, 16, 434–439.

Manga, M. (2001) Origin of post-seismic streamflow changes inferred from baseflow recession and magnitude-distance relation, Geophys.Res. Lett., 28, 2133–2136, doi:10.1029/2000GL012481.

Manga, M., Brodsky E. E., Boone M. (2003) Response of streamflow to multiple earthquakes and implications for the origin of postseismic discharge changes, Geophys. Res. Lett., 30, 1214, doi:10.1029/2002GL016618.

Manga, M., Rowland J. C., (2009) Response of Alum Rock springs to the October 30, 2007 Alum Rock earthquake and implications for the origin of increased discharge after earthquakes, Geofluids, 9(3), 237–250.

Manga, M., Beresnev I., Brodsky E. E., Elkhoury J. E., Elsworth D., Ingebritsen S. E., Mays D. C., Wang C. Y. (2012) Changes in permeability caused by transient stresses: Field observations, experiments,and mechanisms, Rev. Geophys., 50, RG2004, doi:10.1029/2011RG00038.

Ma, Y., Huang, F. (2017) 'Coseismic water level changes induced by two distant earthquakes in multiple wells of the Chinese mainland', Tectonophysics, 694(5), 57–68. doi: 10.1016/j.tecto.2016.11.040.

Mogi, K., Mochizuki, H., Kurokawa, Y. (1989) Temperature changes in an artesian spring at Usami in the Izu Peninsula (Japan) and their relation to earthquakes. Tectonophysics, 159(1), 95–108.

Muir-Wood, R., King G. C. P., (1993) Hydrological signatures of earthquake strain, J. Geophys. Res., 98, 22035–22068, doi:10.1029/93JB02219.

Rojstaczer, S., Wolf S., Michel R. (1995) Permeability enhancement in the shallow crust as a cause of earthquake-induced hydrological changes, Nature, 373, 237–239.

Roeloffs, E. A. (1996) Poroelastic techniques in the study of earthquakes-related hydrologic phenomena. Adv Geophys 37(1):135–195

Roeloffs, E. A. (1998) Persistent water level changes in a well near Parkfield, California, due to local and distant earthquakes, J. Geophys. Res., 103, 869–889, doi:10.1029/97JB02335.

Shi, Z., Wang G. (2014) Hydrological response to multiple large distant earthquakes in the Mile well, China. J. Geophys. Res. Earth Surf. 11, 2448–2459.

Shi, Y.L., Cao, J.L., Ma, L., (2007) Tele-seismic coseismic well temperature changes and their interpretation. Acta Seismologica Sinica 29 (3), 265–273.

Shi, Z., Wang G., Manga M., Wang C.-Y. (2015b) Mechanism of coseismic water level change following four great earthquakes—Insights from coseismic responses throughout the Chinese mainland, Earth Planet. Sci. Lett., 430, 66–74.

Shi, Z., Wang G., Manga M., Wang C.-Y. (2015) Mechanism of co-seismic water level change following four great earthquakes—Insights from co-seismic responses throughout the Chinese mainland, Earth Planet. Sci. Lett., 430, 66–74.

Shi, Z., Wang G. (2016) Aquifers switched from confined to semiconfined by earthquakes, Geophys. Res. Lett., 43,11,166–11,172, doi:10.1002/2016GL070937.

Sibson, R. H., Rowland J. V. (2003) Stress, fluid pressure and structural permeability in seismogenic crust, North Island, New Zealand, Geophys. J. Intl., 154, 584–594, doi:10.1046/j.1365-246X.2003.01965.x.

Skelton, A., Andrén, M., Kristmannsdóttir, H. et al. (2014) Changes in groundwater chemistry before two consecutive earthquakes in Iceland, Nat. Geosci., 7, 752–756.

Sun, X., Wang, G., Yang, X. (2015) 'Coseismic response of water level in Changping well, China, to the Mw 9.0 Tohoku earthquake', Journal of Hydrology, 531, 1028-1039.

Shi, Z., Wang G., Wang C.-Y., Manga M., Liu C. (2014) Comparison of hydrological responses to the Wenchuan and Lushan earthquakes, Earth Planet. Sci. Lett., 391, 193–200.

Shi, Z., Wang G. (2014) Hydrological response to multiple large distant earthquakes in the Mile well, China, J. Geophys. Res. Earth Surf., 119, 2448–2459.

Shi, Z., Wang G. (2015) Sustained groundwater level changes and permeability variation in a fault zone following the 12 May 2008, Mw 7.9 Wenchuan earthquake, Hyrol. Processes, 29(12), 2659–2667.

Tamura, Y., Sato T., Ooe M., Ishiguro M. (1991) A procedure for tidal analysis with a Bayesian information criterion, Geophysical Journal International, 104(3), 507–516.

Toda, S., Stein, R.S., Richards-Dinger, K., et al. (2005) Forecasting the evolution of seismicity in southern California: animations built on earthquake stress transfer. J. Geophys. Res.110, B05S16.

Wang, C.-Y. (2007) Liquefaction beyond the near field, Seismol. Res. Lett., 78, 512–517.

Wang, C.-Y., Manga M. (2015) New streams and springs after the 2014 Mw6. 0 South Napa earthquake, Nat. Commun., 6, 7597, doi:10.1038/ncomms8597.

Wang, C.-Y., Wang C.-H., Manga M. (2004a) Coseismic release of water from mountains: Evidence from the 1999 (Mw = 7.5) Chi-Chi,Taiwan, earthquake, Geology, 32, 769–772, doi:10.1130/G20753.1.

Wang, C.-Y., Manga M., Dreger D., Wong A. (2004b) Streamflow increase due to rupturing of hydrothermal reservoirs: Evidence from the 2003 San Simeon earthquake, California, earthquake, Geophys. Res. Lett., 31, L10502, doi:10.1029/2004GL020124.

Wang, C.-Y. (2007) Liquefaction beyond the near field, Seismol. Res. Lett., 78, 512–517.

Wang, C.-Y., Wang L.-P., Manga M., Wang C.-H., Chen C.-H. (2013) Basin-scale transport of heat and fluid induced by earthquakes, Geophys. Res. Lett., 40, 3893–3897, doi:10.1002/grl.50738

Wang, C.-Y., Manga M. (2015) New streams and springs after the 2014 M6.0 South Napa earthquake, Nat. Commun., 6, 7597.

Wang, C.-Y., Doan M.-L., Xue L., Barbour, A. J. (2018) Tidal response of groundwater in a leaky aquifer—Application to Oklahoma. Water Resources Research, 54, 8019–8033.

Wang, C. - Y., Zhu, A. - Y., Liao, X., Manga, M., Wang, L. - P. (2019) Capillary effects on groundwater response to Earth tides. Water Resources Research, 55, 6886–6895.

Xue, L., Li H.-B., Brodsky E. E., Xu Z.-Q., Kano Y., Wang H., Mori J. J., Si J.-L., Pei J.-L., Zhang W. (2013) Continuous permeability measurements record healing inside the Wenchuan earthquake fault zone, Science, 340(6140), 1555–1559.

Yan, R., Woith H., Wang R. (2014) Groundwater level changes induced by the 2011 Tohoku earthquake in China mainland, Geophys. J. Int., 199(1), 533–548.

Zhang, Y., Fu L., Ma Y., Hu J. (2016) 'Different hydraulic responses to the 2008 Wenchuan and 2011 Tohoku earthquakes in two adjacent far-field wells: The effect of shales on aquifer lithology 4. Seismology', Earth, Planets and Space, 68, 17, doi: 10.1186/s40623-016-0555-5.

Zhang, Y., Wang C.-Y., Fu L.-Y., Zhao B., Ma Y., Unexpected far-field hydrological response to a great earthquake, Earth and Planetary Science Letters, 519, 202–212.

Zeng, X., Lin,Y., Chen W., Bai Z., Liu J.Y., Chen, C.H., 2014. Multiple seismo-anomalies associated with the M6.1 Ludian earthquake on August 3, 2014, Journal of Asian Earth Sciences, 114, 352–361.

Figures

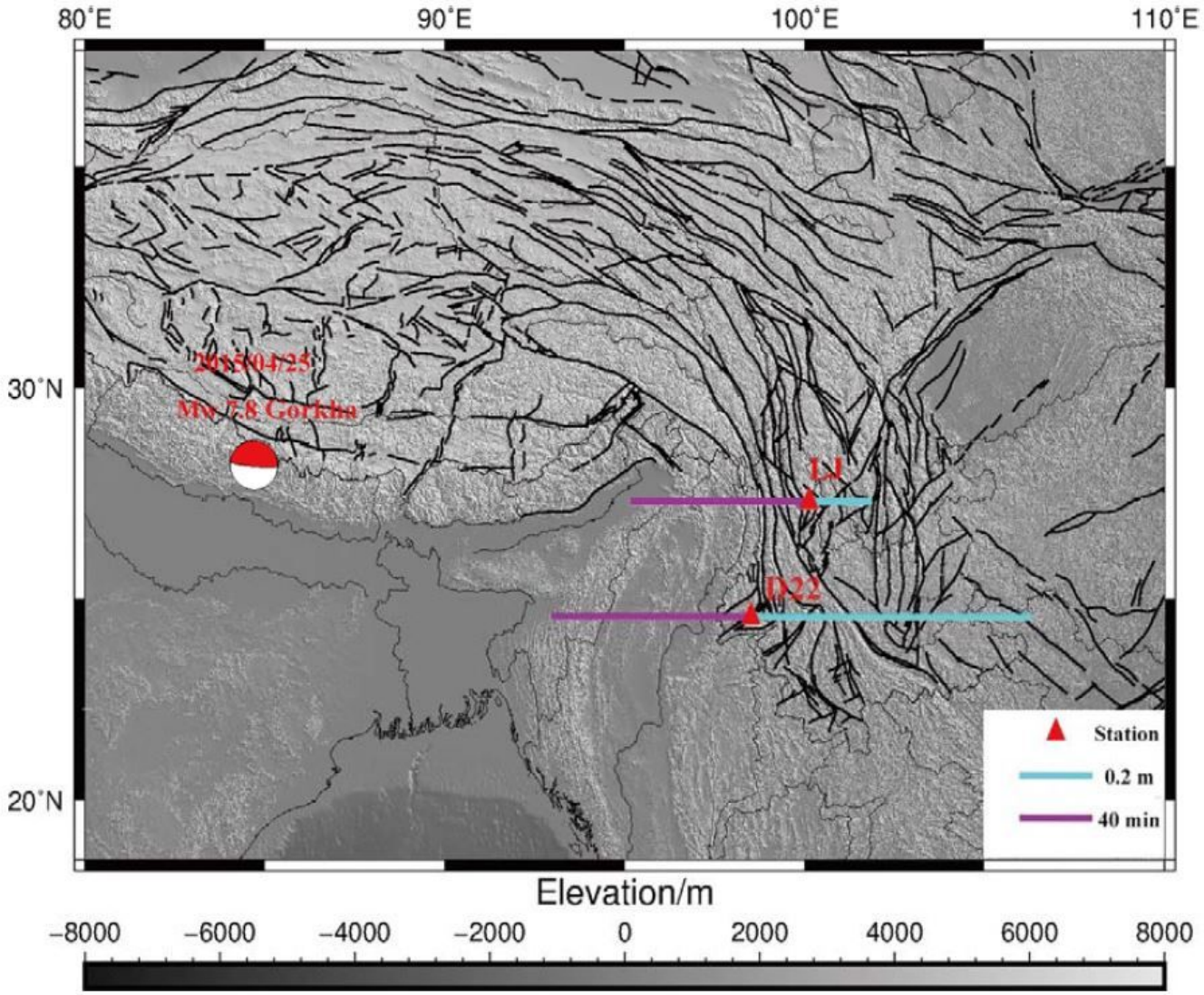

Figure 1

Map showing the locations of the MS well and LJ well (red solid triangles). ‘Beach ball’ shows the epicenter and focal mechanism of the 2015 Mw 7.8 Gorkha earthquake (Avouac et al., 2015). Black lines denote the location of surface faults on the Chinese mainland (Deng et al. 2006). The blue and purple lines indicate the variation amplitude and duration of water level responses to The Gorkha earthquake respectively.

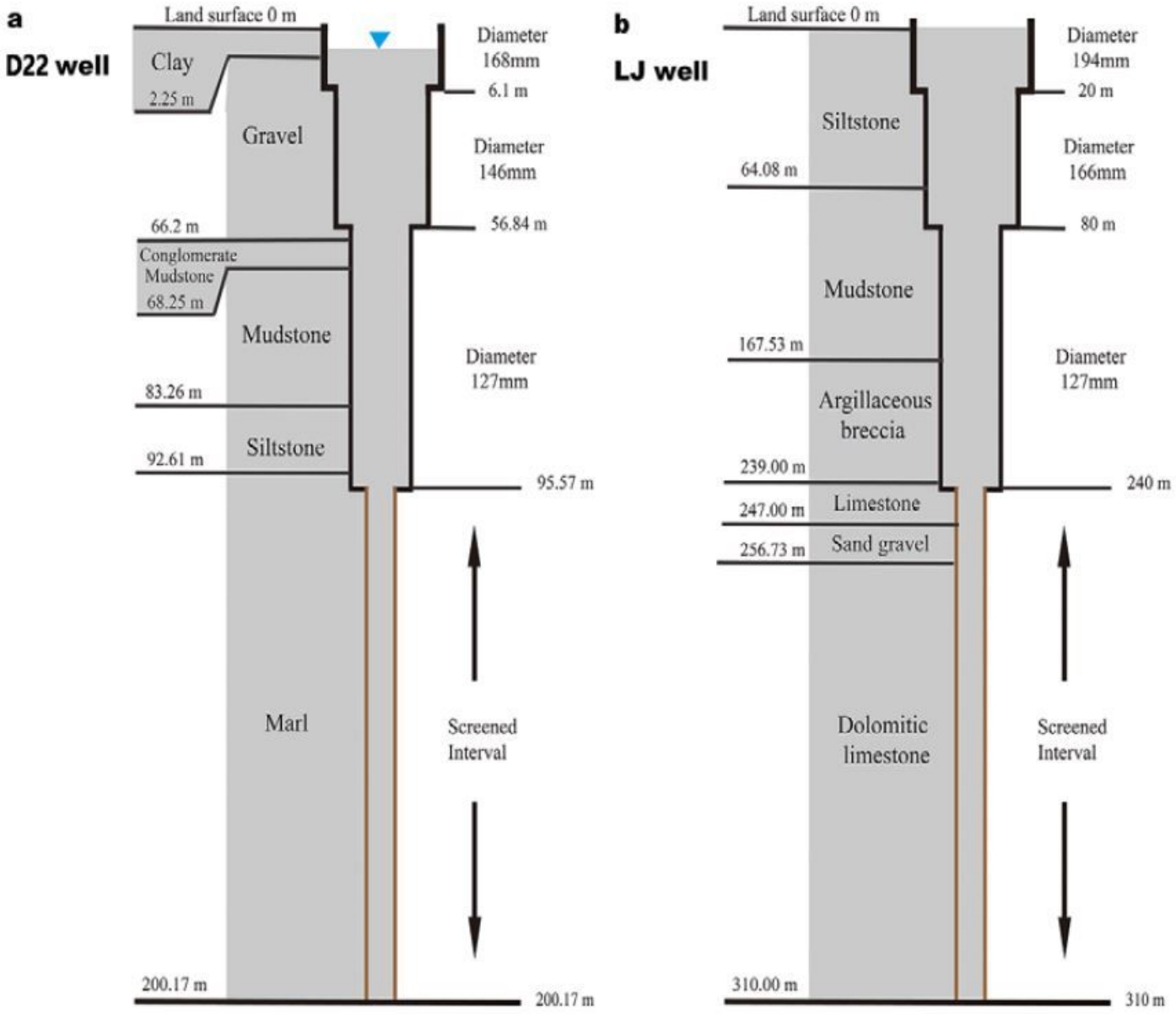

Figure 2

Wellbore structure and lithology of the MS well a) and LJ well b)

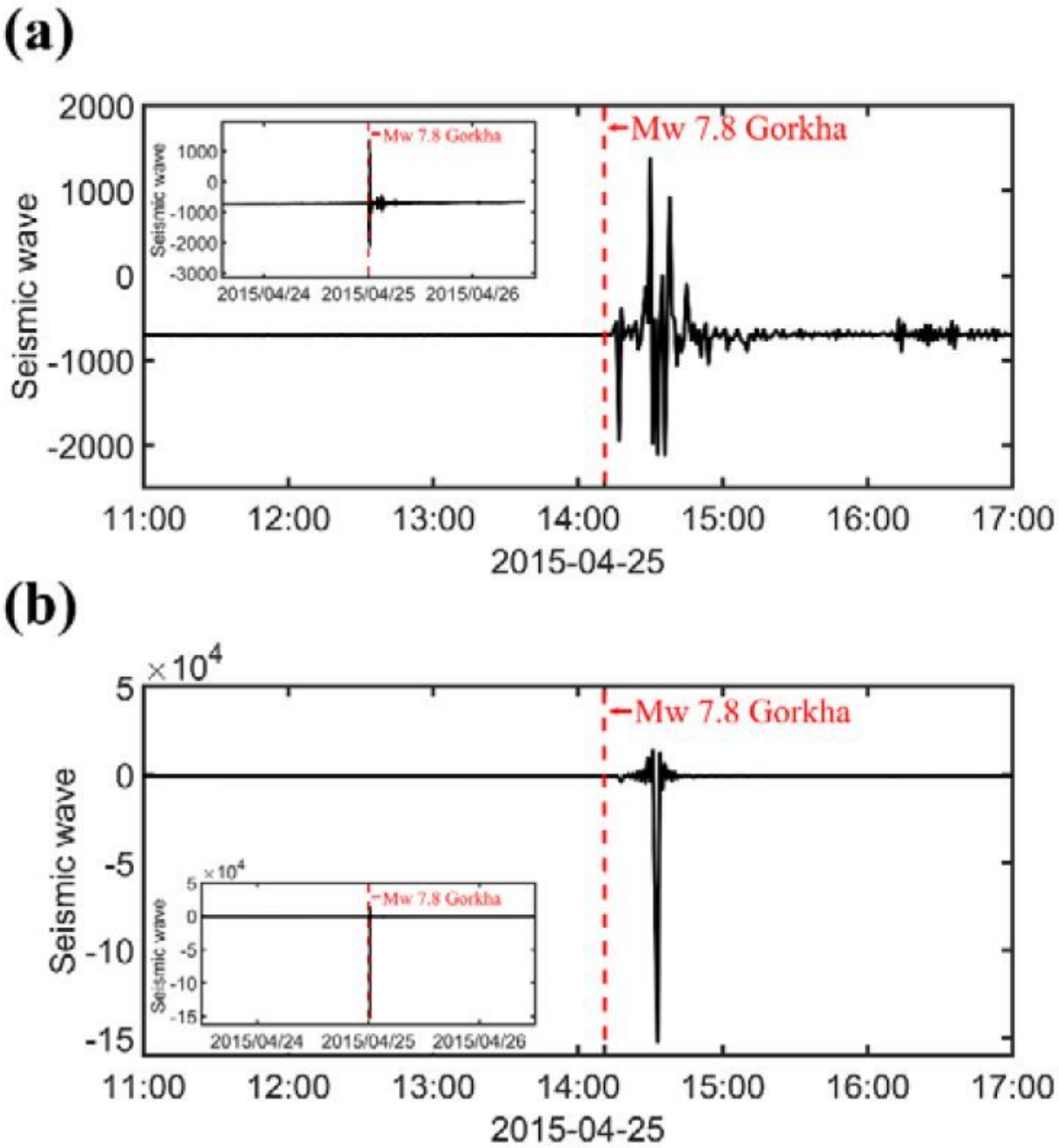

Figure 3

Z-component seismic wave records of displacement at the MS (a) and LJ (b). The red dotted lines represent the earthquake origin time. The unit is nm.

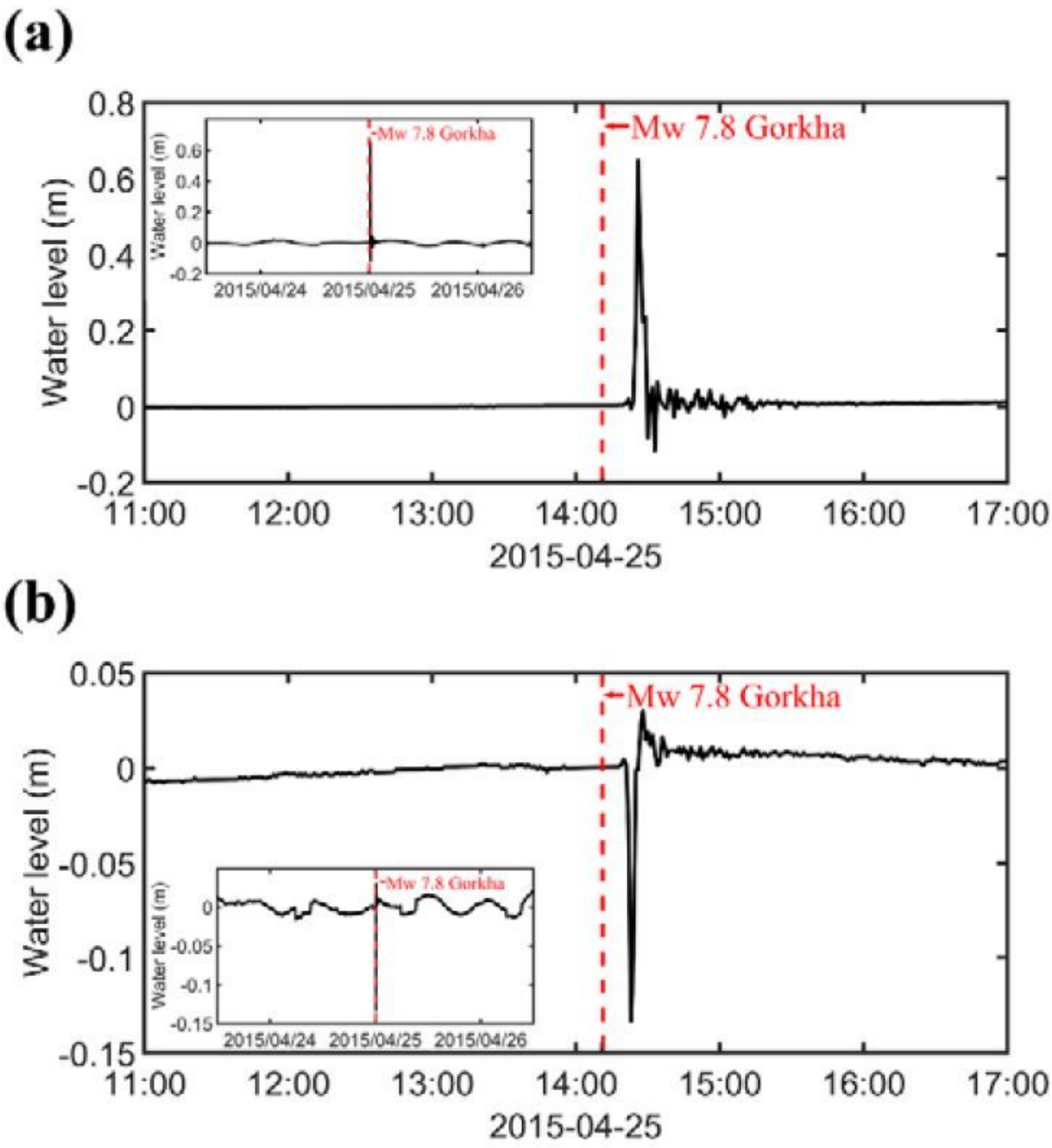

Figure 4

Water levels at the MS (a) and LJ (b). The red dotted lines represent the earthquake origin time.

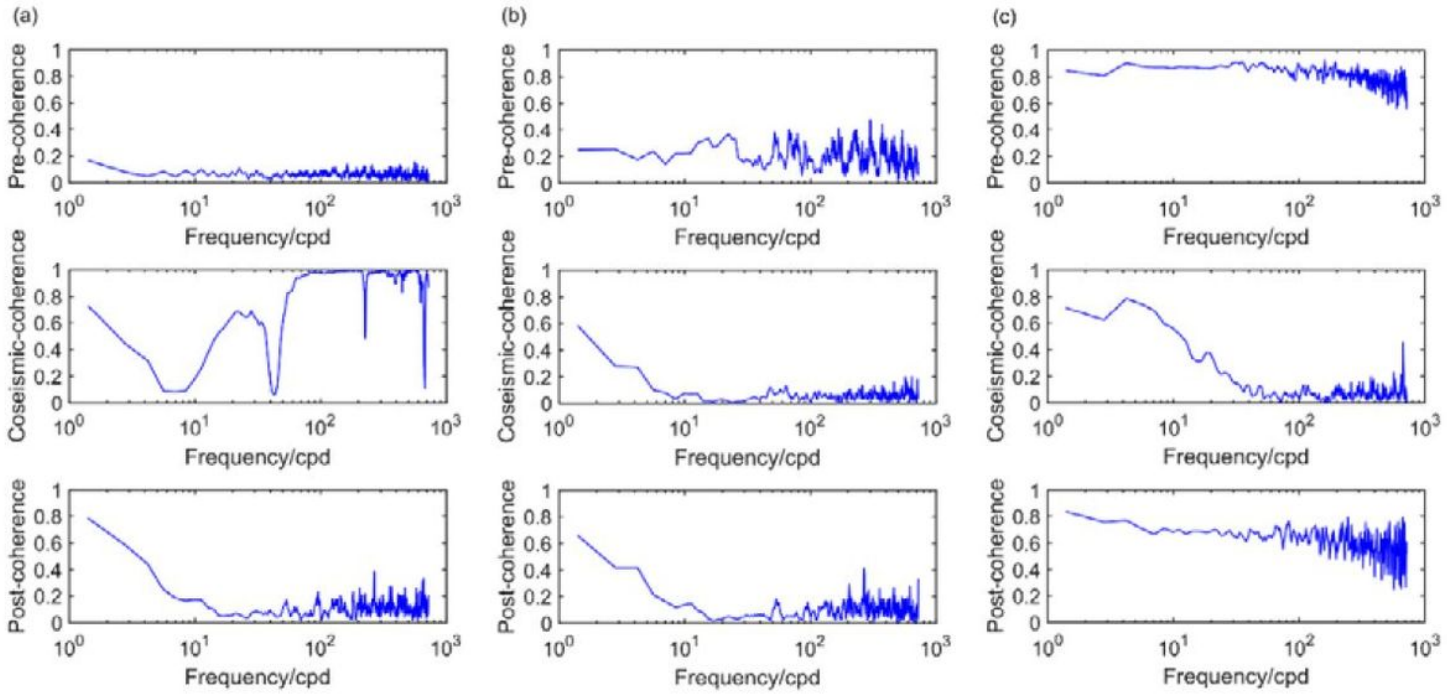

Figure 5

Gorkha earthquake preseismic, coseismic and postseismic coherences between water level and vertical displacement (a), barometric pressure and vertical displacement (b), as well as water level and barometric pressure (c) in the D22 well.

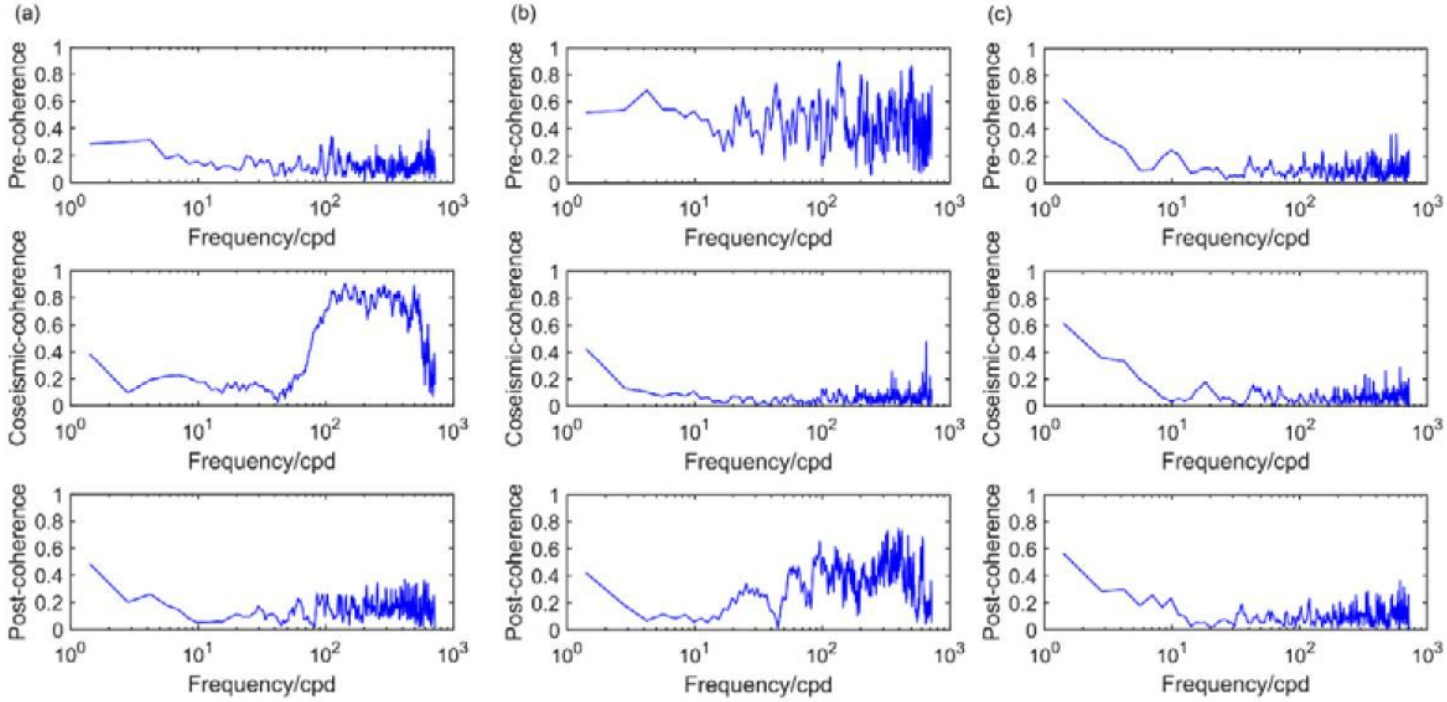

Figure 6

Gorkha earthquake preseismic, coseismic and postseismic coherences between water level and vertical displacement (a), barometric pressure and vertical displacement (b), as well as water level and barometric pressure (c) in the LJ well.

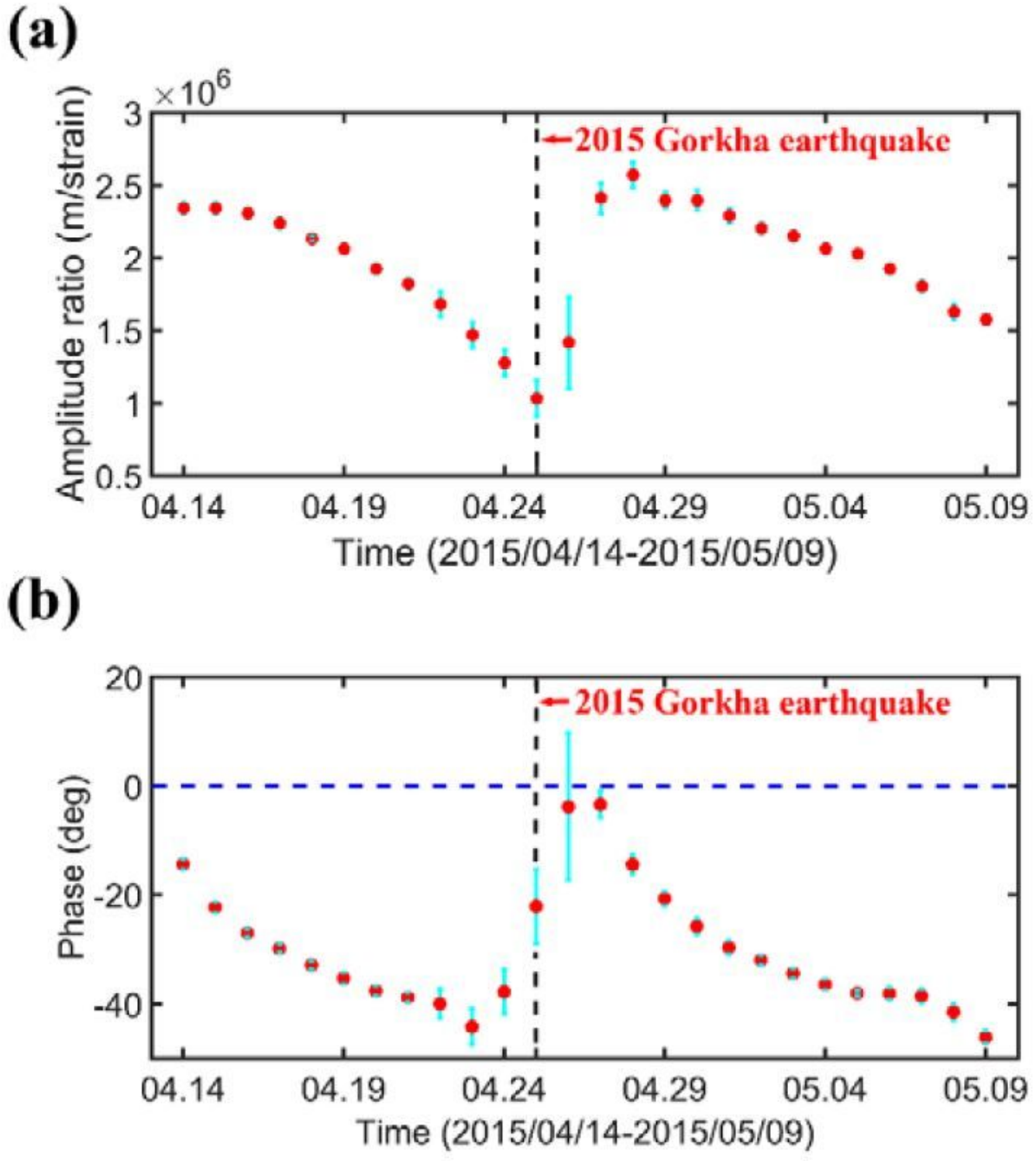

Figure 7

amplitude ratio and phase response of D22 well under M2 wave frequency change with time, and amplitude response is amplitude ratio of earth tide water level. Dotted line shows the start time of 2015

Gorkha earthquake (Beijing time, see Figure 3). The blue error bars indicate the root-mean-square error (RMSE) of the tidal analysis.

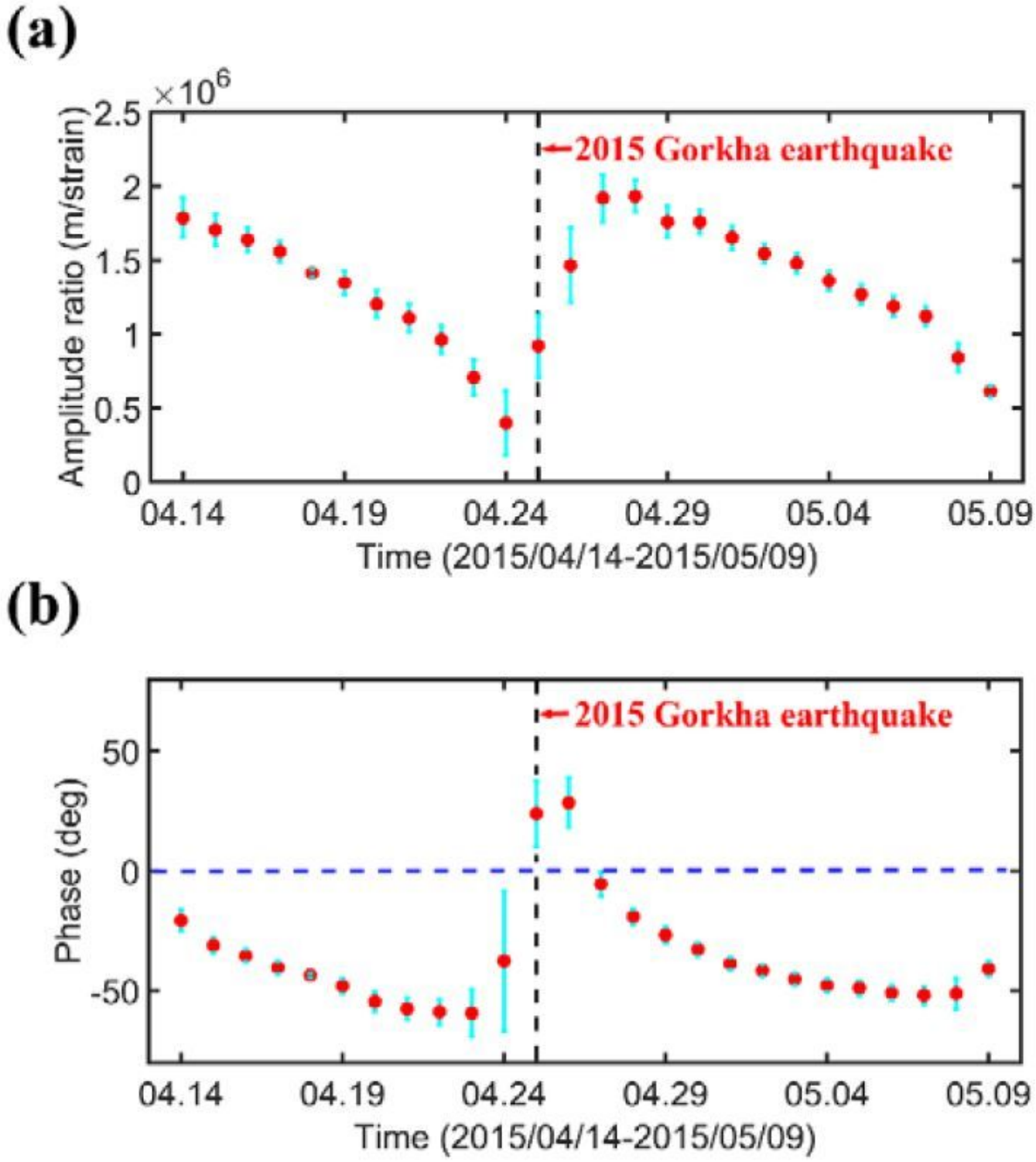

Figure 8

amplitude ratio and phase response of LJ well change with time under M2 wave frequency, and amplitude response is amplitude ratio of earth tide water level. Dotted line shows the start time of 2015

Gorkha earthquake (Beijing time). The blue error bars indicate the root-mean-square error (RMSE) of the tidal analysis.

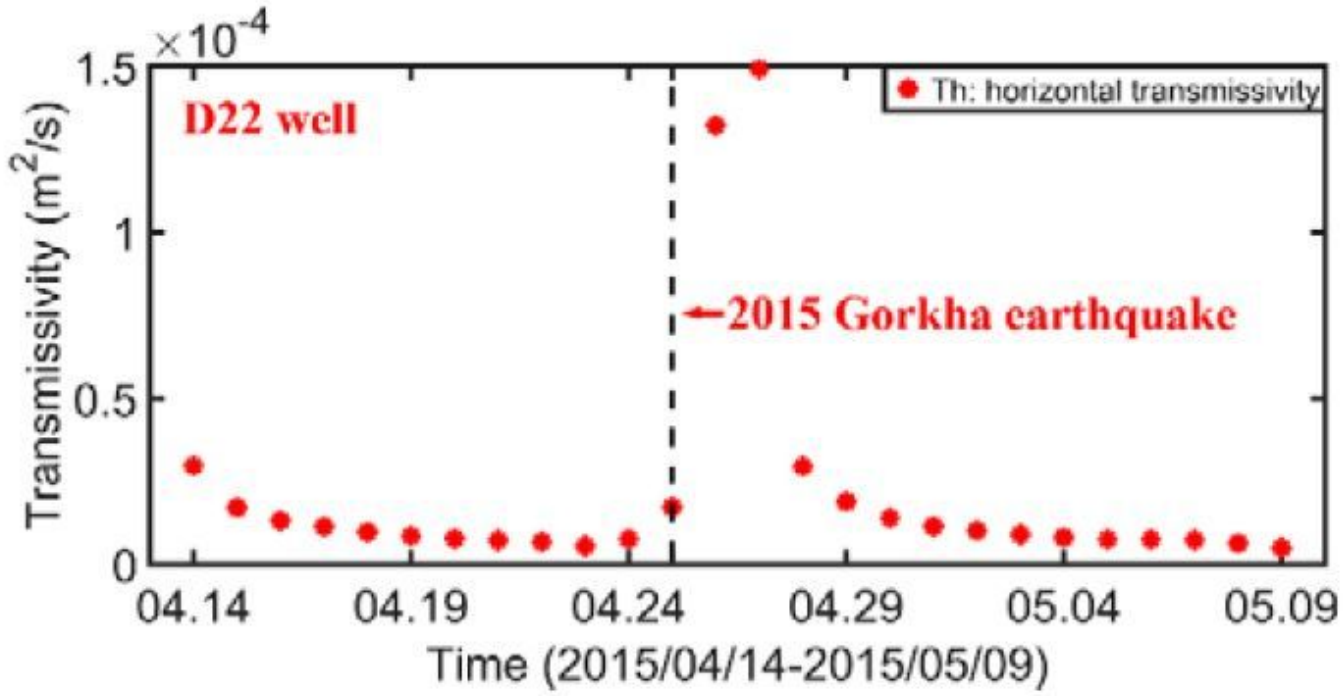

Figure 9

Time dependent transmissivity (Th) of the D22 well based on M2 tide analysis. Dotted line shows the origin time of 2015 Gorkha earthquake.

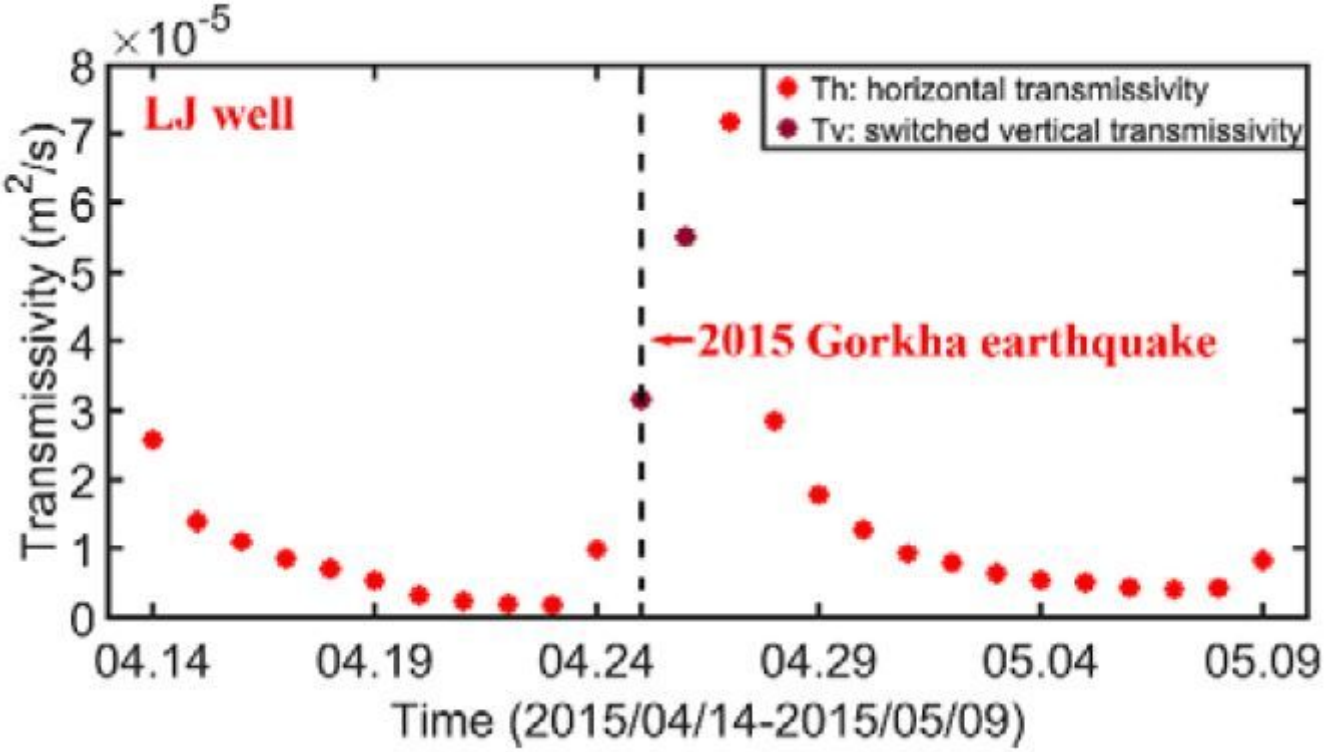

Figure 10

Time dependent transmissivity (Th switches to Tv, and restores.) of the LJ well based on M2 tide analysis. Dotted line shows the origin time of 2015 Gorkha earthquake. Th is calculated from the Hsieh's horizontal flow model and Tv calculated from the vertical pore-pressure diffusion model.

Supplementary Files

This is a list of supplementary files associated with this preprint. Click to download.

- GrapghAbstract.tif
- f9.tif
- f8.tif
- f7.tif
- f6.tif
- f5.tif
- f4.tif
- f3.tif
- f2.tif
- f10.tif
- f1.tif